Optical and microstructural characterization of porous silicon using photoluminescence, SEM and positron annihilation spectroscopy

2007 J. Phys.: Condens. Matter 19 486002

(http://iopscience.iop.org/0953-8984/19/48/486002)

IOP PUBLISHING JOURNAL OF PHYSICS: CONDENSED MATTER

J. Phys.: Condens. Matter **19** (2007) 486002 (17pp) doi:10.1088/0953-8984/19/48/486002

Optical and microstructural characterization of porous silicon using photoluminescence, SEM and positron annihilation spectroscopy

C K Cheung[1], F Nahid[1], C C Cheng[1], C D Beling[1], S Fung[1], C C Ling[1], A B Djurišić[1], C Pramanik[2], H Saha[2] and C K Sarkar[2]

[1] Department of Physics, The University of Hong Kong, Pokfulam Road, Hong Kong
[2] Department of Electronics and Telecommunication Engineering, Jadavpur University, Kolkata 700032, India

Received 17 June 2007, in final form 4 October 2007
Published 5 November 2007
Online at stacks.iop.org/JPhysCM/19/486002

Abstract

We have studied the dependence of porous silicon morphology and porosity on fabrication conditions. N-type (100) silicon wafers with resistivity of 2–5 Ω cm were electrochemically etched at various current densities and anodization times. Surface morphology and the thickness of the samples were examined by scanning electron microscopy (SEM). Detailed information of the porous silicon layer morphology with variation of preparation conditions was obtained by positron annihilation spectroscopy (PAS): the depth-defect profile and open pore interconnectivity on the sample surface has been studied using a slow positron beam. Coincidence Doppler broadening spectroscopy (CDBS) was used to study the chemical environment of the samples. The presence of silicon micropores with diameter varying from 1.37 to 1.51 nm was determined by positron lifetime spectroscopy (PALS). Visible luminescence from the samples was observed, which is considered to be a combination effect of quantum confinement and the effect of Si=O double bond formation near the SiO_2/Si interface according to the results from photoluminescence (PL) and positron annihilation spectroscopy measurements. The work shows that the study of the positronium formed when a positron is implanted into the porous surface provides valuable information on the pore distribution and open pore interconnectivity, which suggests that positron annihilation spectroscopy is a useful tool in the porous silicon micropores' characterization.

1. Introduction

Porous silicon was first reported in 1956 by Uhlir in the study of electropolishing of silicon using hydrofluoric acid [1]. The discovery of photoluminescence from porous silicon in 1990 by Canham [2] resulted in a great deal of interest in studying this material because of its efficient visible luminescence, flexibility to control and potential application in silicon-based optoelectronics systems [3, 4]. A variety of spectroscopy techniques have been used

in the understanding of its structural and optical properties including photoluminescence spectroscopy [2], x-ray diffraction [5], secondary electron microscopy (SEM) [6] and Raman spectroscopy [7]. It has been shown to have efficient luminescence in a range extending from the near-infrared [8] to the blue region of the visible spectrum [9]. Red light emission can normally be achieved in a freshly grown sample while blue luminescence only occurs in oxidized porous silicon [10, 11]. To date, the mechanism of the luminescence properties of porous silicon is widely believed to be the result of the quantum confinement of carriers in crystalline Si wires [2, 12]. However, it was reported that quantum confinement alone cannot explain the redshift of the PL for blue luminescent samples with pore sizes smaller than 3 nm [13, 14] so that the additional influence of the surface coverage (such as oxygen or impurities) has to be considered. Porous silicon has been extensively studied in the last decade, while the exact microstructure of this material has not yet been completely characterized and there is still no obvious way of measuring the micropore porosity reliably [15–17]. New characterization methods are thus necessary for the micropore size characterization.

The use of positron annihilation spectroscopy (PAS) in porous silicon was first reported by Ito *et al* [18] in 1993, who found a long positron lifetime component of several tens of nanoseconds in a positron lifetime study. The long lifetime component was confirmed to be due to the existence of positronium (Ps) from two-dimensional angular correlation of annihilation radiation (ACAR) spectra, from which a narrow peak was observed [19]. Knights *et al* [20] used a positron beam to study porous silicon and to find a short positron diffusion length. These observations indicated a strong positron trapping in the porous layer. A monoenergetic pulsed positron beam was used by Suzuki *et al* to study the behavior of Ps in porous silicon at various annealing temperatures [21]. They found that the long-lived positron lifetime component was strongly dependent on the annealing temperature. The samples annealed at 200–400 °C showed a significantly higher *o*-Ps intensity than that of the initial sample and they suggested that this increase was due to the contribution of micro-structural relaxation. Dannefaer *et al* [22] studied the effect of heat treatment of porous silicon under an argon ambient and they found that the treatment increased both the mass of the porous film and increased the volume of defects. These pioneering works have shown the potential of characterizing porous silicon through the study of Ps formed near the surface.

In this paper, various techniques are applied in the characterization of porous silicon. The aim is to study the microstructural properties of porous silicon using PAS and correlate with its optical properties. In particular, SEM and slow positron beam spectroscopy are used to study the surface of porous silicon samples. SEM images are used for characterizing the surface morphology. The positron beam technique is used to study the depth-defect profile and the characteristics of the open pores through the variations in the positronium fraction with varying incident positron energy. Evidence is given that positronium diffusion lengths can help study the connectivity of the open pores in porous silicon. In addition, the positron annihilation lifetime spectroscopy (PALS) technique is employed to study the average pore size distribution of the porous layer. The chemical environment of the porous silicon after anodization is studied using the coincidence Doppler broadening spectroscopy (CDBS) technique. Photoluminescence studies are also performed to provide additional information on the optical properties of the Si nanocrystalline structure.

2. Background theory: the positron porosimetry technique

PAS has been proven to be a useful tool in open volume defects in semiconductors [23]. This technique utilizes the sensitivity of positrons to the electron momentum density and distribution of the material. By implanting a positron into condensed matter, it annihilates with an electron

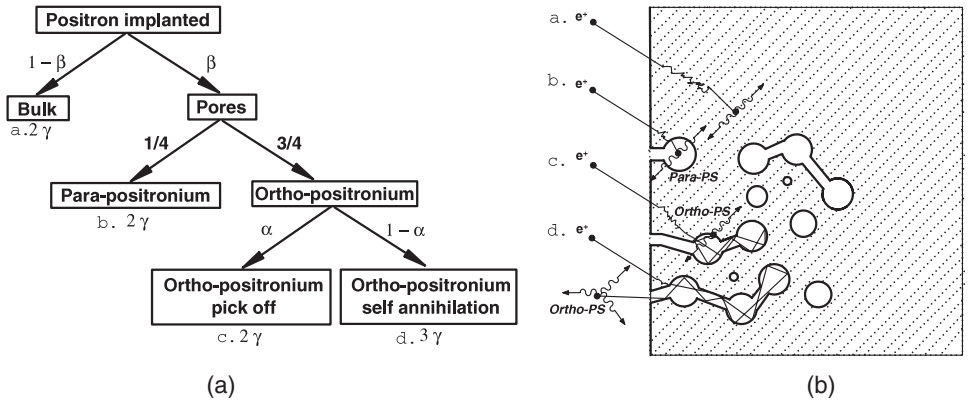

Figure 1. Diagrams showing possible fates of positronium. (a) Time development, (b) in real space.

and two γ rays with energy 511 keV are emitted. The motion of the positron–electron pair not only produces a small angle deviation from collinearity between the two 511 keV photons but also a Doppler shift to the annihilation radiation. The fact that these annihilation parameters in defects are different from a defect-free bulk state allows PAS to be a direct method of identifying point defects. The Doppler shift can be measured using a high resolution Ge detector. The observables commonly used in representing the shift are the lineshape parameter S and the wing parameter W. The S parameter is the fraction of the central region that is sensitive to the annihilation of positrons with the low momentum valence electron and the W parameter is the fraction of the two wing regions of the 511 keV photopeak that reflects the positron annihilation with core electrons.

Recently, PAS has been shown to be a useful non-destructive method for the characterization of open and close porosity in porous media [24, 25]. The pore structure and their morphology can be determined by interpreting the way that positron and positronium annihilate in porous materials. Considerable success has been shown over the past decade in the characterization of porous material with pore sizes and distributions in the range of 0.3–30 nm by the positronium lifetime and the $3\gamma/2\gamma$ technique [26–28]. These techniques offer the possibility of investigating some important properties of porous materials such as the pore size, porosity and interconnectivity.

The fate of positronium atoms formed in porous material is shown schematically in figure 1. The positron implanted in the material is thermalized and has its energy lowered to a few electron volts. Positronium may be formed by the positron capturing a bound molecular electron or recombining with a free 'spur' electron generated by ionizing collisions. The positronium atoms formed are thus p-Ps and o-Ps and once formed they begin to diffuse and thermalize in the material. p-Ps has a short lifetime (125 ps) because the positron in the p-Ps predominantly undergoes 2γ annihilation with its bound electron. The o-Ps formed has intrinsically a much longer lifetime (142 ns). As such it can more readily localize in a pore, thermalize and finally annihilate with molecularly bound electrons through the 'pick-off' process. 'Pick-off' annihilation is a 2γ process that can decrease the Ps lifetime to values as low as $\sim$1 ns. The o-Ps may also diffuse over long distances if pores are interconnected with the possibility of exiting into the surrounding vacuum and undergoing 3γ annihilation with a characteristic lifetime of 142 ns. The analysis of the fate of the positronium can provide valuable information in the characterization of porous materials. To date, two major techniques

have been employed for such analysis, namely the $3\gamma/2\gamma$ ratio technique and the positronium lifetime technique.

2.1. The $3\gamma/2\gamma$ ratio technique

The three-body (photon) annihilation of *o*-Ps contributes a characteristic decay spectrum ranging from 0 to 511 keV because the sum of the energy of any pair of photons must be less than $m_e c^2$ through momentum conservation. This is in contrast to the case of two gamma decay which leads to nearly monoenergetic photons having an energy of $m_e c^2$. The result is that, when more *o*-Ps annihilation occurs, the region of the spectrum below 511 keV increases in intensity while the 511 keV annihilation peak decreases in intensity. To determine the fraction of *o*-Ps, F, produced at the surface of the sample, the total valley spectrum counts T and the photo-peak counts P were measured. P and T are given by [29]

$$P = N(1-F)g_{2\gamma} + \tfrac{3}{4}NFg_{3\gamma} + \tfrac{1}{4}NFg_{2\gamma} \tag{1}$$

$$T = N(1-F)h_{2\gamma} + \tfrac{3}{4}NFh_{3\gamma} + \tfrac{1}{4}NFh_{2\gamma}, \tag{2}$$

where N is the total number of positrons per second entering the sample, $g_{2\gamma}$ and $g_{3\gamma}$ are the probabilities of a 2γ and 3γ annihilation event contributing to the peak region respectively and $h_{2\gamma}$ and $h_{3\gamma}$ are the probabilities of a 2γ and 3γ annihilation event contributing to the total region. By defining the 3γ to 2γ annihilation ratio ('R' parameter) as [29]

$$R = \frac{(T-P)}{P} \tag{3}$$

and substituting equations (1) and (2) and solving for F, we have [29]

$$F = \left[1 + \frac{P_1}{P_0}\left(\frac{R_1 - R}{R - R_0}\right)\right]^{-1}, \tag{4}$$

where the subscripts 0 and 1 denote values corresponding to the 0% and 100% Ps formation, respectively.

2.2. Positronium lifetime technique

Positron lifetime spectroscopy is one of the most widely used methods for characterizing polymer and porous materials [25]. The *o*-Ps lifetime component resolved from the positron lifetime is capable of determining size, structure and relative fraction of free volume in porous materials. The size of the free volume with spherical geometry in the porous material may be estimated from the relation [30, 31]:

$$1/\tau = 2[1 - r/r_0 + (1/2\pi)\sin(2\pi r/r_0)] \tag{5}$$

with τ being the *o*-Ps lifetime in ns and r_0 is the radius of the spherical pore that is equal to $r + \delta r$. Here δr is an empirical parameter and equal to 0.1656 nm as obtained by fitting the observed lifetimes with the known pore sizes in molecular substrates [32]. The equation can also been modified for the determination of open volume pores with nonspherical geometries [33], but the parameters obtained do not have a significant difference resulting from difference geometry. The intensity of the *o*-Ps lifetime I_3 may also be used to obtain information about the relative numbers of free volume sites [34, 35]

3. Experiment

In the present study, porous silicon samples have been fabricated by etching n-type silicon wafers having resistivity 2–5 Ω cm and (100) orientation. All the as-cut wafers have been

polished by a standard anisotropic alkali etching method (20% KOH solution, 70 °C, 5 min). Back metal contacts were established by the screen-printing of Ag–Al paste and its subsequent firing at 700 °C (45 s). The screen-printed silicon wafers were anodized in a Teflon cell specially developed for the purpose [36]. The wafers act as a seal between the front and the rear regions. The front and the rear regions are filled with a mixture of HF–CH_3OH (1:1) and dilute KCl (5%) solution, respectively. The back contact, which was in contact with the KCl solution, was connected to the positive terminal of a power supply by a platinum electrode. The front surface of the wafer was exposed to the HF–CH_3OH electrolyte. A platinum rod was used as the cathode. The samples were then anodized by a constant current power supply in the presence of illumination. The current density and anodization time were varied so that four samples with different porosity and film thickness were obtained.

The thickness and the surface morphology of the porous layers were examined using a Leo 1530 field emission SEM. The EDAX Phoenix EDS system equipped in the SEM facility was used in the elemental analysis and mapping of the samples surfaces. The slow positron beam at HKU [37] was then used to study the surface parameters via variable energy Doppler broadening spectroscopy (VEDBS) and 3γ-to-2γ ratio measurements. The positron beam was focused to ∼1 mm and the beam energy varied from 0.2 to 26 keV. 3×10^6 events were acquired at each selected beam energy. The open porosity and pore connectivity of the studied samples were evaluated by studying the fraction of *o*-Ps escaping from the sample into vacuum. This was done by determining the R parameter as a function of the positron implantation energy. The counts T of the valley were taken in the region 410 keV $\leqslant E_\alpha \leqslant$ 500 keV and the peak count region is taken as 511 ± 9 keV. The positronium fraction F was determined using equation (4). The value of R_1 (100% positronium formation) was taken as the value of R obtained by extrapolating to zero implantation energy and R_0 (0% positronium formation) as the R value obtained at the highest implanted positron energy. Standard VEDBS spectra were also acquired by the variation of the low momentum 'S' parameter with beam energy. The S parameter calculated is defined as the ratio of the count in the photopeak in the energy range of 511 ± 0.85 keV to the total area of the peak (511 ± 5 keV).

The chemical environment and the pore size distribution of the porous silicon layer prepared under different anodization conditions were then studied using the coincidence Doppler broadening spectroscopy (CDBS) and the positron annihilation lifetime spectroscopy (PALS) techniques, respectively. The positron source used here was a Na^{22} source embedded between two aluminum foils and the sample–source assembly was prepared in the 'sandwich' configuration. The CDBS system used in this work comprised of two high purity Ge detectors with resolutions of 1.1 and 1.3 keV measured at 514 keV. The energies of the annihilation photons were digitized using two 8713 ADCs and were processed using the FastComTec MPAIII multi-parameter system with a 2 μs resolution time. CDBS spectra were collected with 10^8 total counts into a 512 × 512 pixel histogram. The low momentum 'S' and high momentum 'W' parameters were obtained from the CDBS raw data. The 'W' parameter is defined as the ratio of the count in the 'Wing' region (507.8–509.3 keV and 512.7–514.8 keV) to the peak total area. For the PALS system, positron spectra were collected through a conventional positron lifetime experiment set-up, having a resolution of ∼224 ps and conversion 12.2 ps/channel. The measurements were performed at room temperature with 2×10^6 counts.

Finally, PL spectroscopy was performed with a HeCd laser (325 nm) as the excitation source to study the optical property of the samples. Luminescence was collected via suitable optics and dispersed using a Spex500M spectrometer. The PL signal emitted in the 320–1000 nm range by the sample at room temperature was collected by a R943 photomultiplier tube and PDA-512-USB (Control Development Inc.) fiberoptic spectrometer.

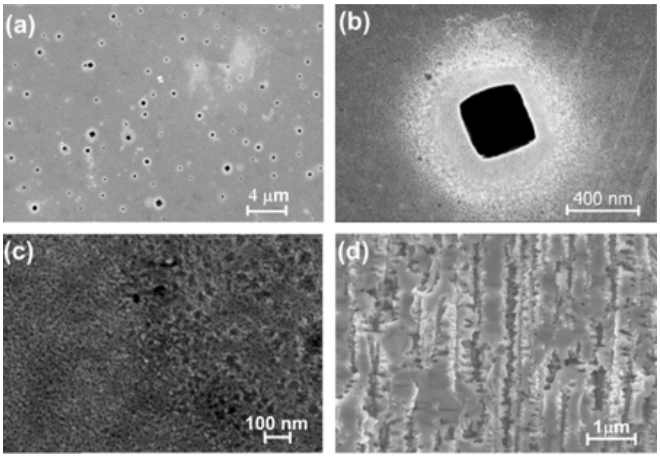

Figure 2. (a)–(c) SEM micrographs of porous silicon obtained from an electrochemically etched n-type silicon wafer, showing the structure and type of the pores formed in the silicon wafer. (d) Cross-sectional SEM image of the porous silicon layer.

4. Result and discussion

4.1. SEM and EDX investigation

In the samples studied, the variation in current density was varied between 20–80 mA cm^{-2} and the etching time between 10–40 min. The thickness of the porous layers was obtained from SEM measurement. The images of the porous silicon sample no. 4 taken by SEM, showing the surface morphology and the cross section of the porous layer, are shown in figure 2. Cross-sectional views of the porous silicon show that the pores propagate along the (100) crystallographic direction, perpendicular to the (100) surface. The thickness of the porous layer increases monotonically from sample 1 to sample 4 with values ∼40 to ∼140 μm, respectively. From the observation of the SEM image on the top surface, the pore shape and spacing exhibit a wide variety of sizes from the nanometer scale to the micron scale. Micropores on the surface are predominantly spherical but square cross sections can be found when the pores size are larger (>200 nm).

EDX analysis was also carried out to examine the chemical composition of the top surface. The results show that the surfaces contain a mixture of silicon and oxygen and the amount of oxygen atoms increases as the etching time and current density increase (table 1). Since the oxygen on the surface should be etched out during the anodization process, the oxygen atom on the sample's surface should be formed after the anodization and when the samples were exposed to ambient air. This is attributed to the increase of surface area exposure to ambient air for the formation of SiO_2 with increasing etching time and current density.

4.2. Positron beam analysis

4.2.1. S parameter analysis. Figure 3 shows the variation of the *S* parameter versus positron implantation energy for the four samples. It can be observed that the *S* parameters of samples 1 and 2 decrease from 0 to 2 keV with a minimum value of ∼0.980 and then increase to a constant value of ∼1.000 as the positron beam energy increases. For samples 3 and 4, however, the *S* parameter tends to first increase (0–1 keV) and then decrease (1–4 keV) with increasing

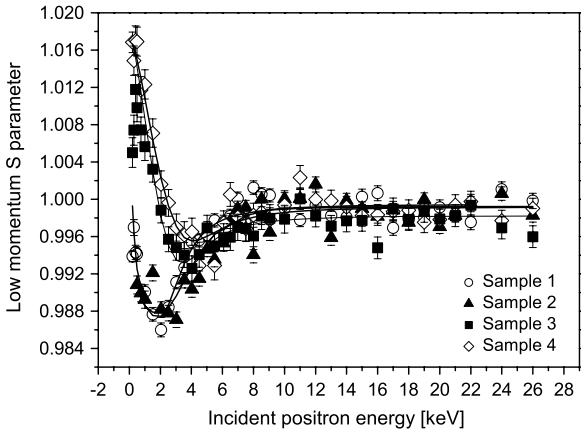

Figure 3. Variation of the *S* parameter versus positron beam energy in the measurement of porous silicon.

Table 1. Conditions for the anodization of n-type silicon wafer, showing variation of current density and etching time. The thickness and the weighting of the chemical compositions of the porous layers were determined by SEM measurement.

Sample number	Current density (mA cm^{-2})	Etching time (min)	Thickness (μm)	O (wt%)	Si (wt%)
1	20	10	36	2.94	97.06
2	40	20	75	8.57	91.43
3	60	30	96	10.68	84.36
4	60	40	146	16.73	79.84

beam energy. In all the samples one finds a lower value of the *S* parameter in the energy range between 2 and 6 keV. The depth profiles of the *S* parameters in all samples remain almost constant at energies higher than 10 keV, which indicates that the majority of the positrons are annihilated in the silicon bulk region. The depth profiling of the *S* parameter has been modeled using the computer program VEPFIT [38] and the fitting results are listed in table 2. The fitting shows that at least a three-layer model is necessary and sufficient for getting a good fit in all the samples. The variation of the *S* parameter in each layer obtained from the program is shown in figure 4. The layers are identified as the silicon oxide layer, the silicon oxide/porous silicon interface and the porous silicon layer. The *S* parameter as a function of the positron implantation energy corresponding to positron–electron annihilation S_{e^+} can be given by a linear combination of *S* parameters in each layer:

$$S_{e^+} = f_{oxy} S_{oxy} + f_{int} S_{int} + f_{Si} S_{Si}, \tag{6}$$

where f_{oxy}, f_{int} and f_{Si} are the fraction of positron–electron 2γ annihilation at the silicon oxide, interface and silicon layers, respectively.

The *S* parameter profile is also affected by the positronium formed near the surface. To have a quantitative study of the measured *S* parameter, the influence of the positronium should be considered [39]. The relationship between the Ps annihilation fraction *F* and *S* parameter at each layer can be analyzed by noting that

$$S = \tfrac{1}{4} F_0 S_{p\text{-Ps}} + \tfrac{3}{4} F_0 S_{o\text{-Ps}} + (1 - F_0) S_{e^+}, \tag{7}$$

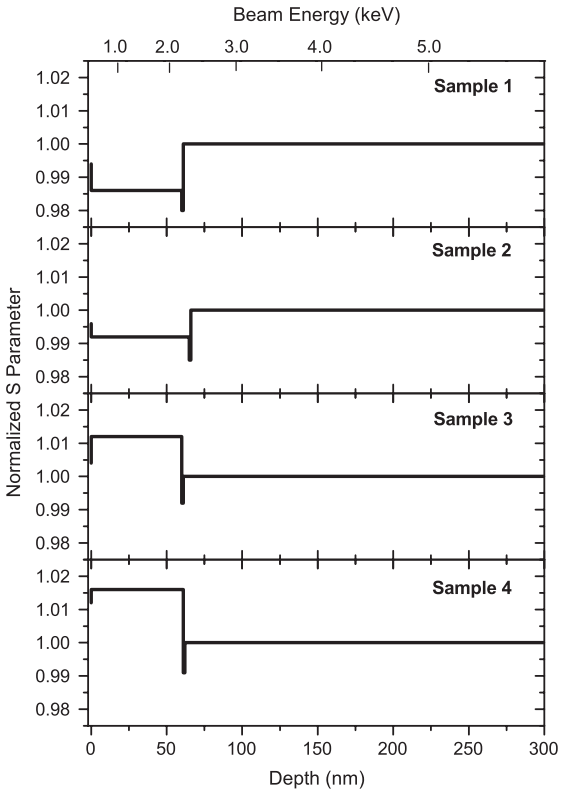

Figure 4. Depth profile of the *S* parameter for the measurement of porous silicon obtained from VEPFIT analysis.

Table 2. Result of the VEPFIT analysis for the porous silicon samples prepared under different anodization current density and time.

Sample	Layer L_i	S_{Li}	S_{surf}	L_+ (nm)	Thickness (nm)
Sample 1	L1	0.986	0.994	7 ± 3	60 ± 1
	L2	0.980		1	1
	L3	1.000		246 ± 39	—
Sample 2	L1	0.992	0.998	64 ± 2	65 ± 1
	L2	0.985		1	1
	L3	1.000		246 ± 39	—
Sample 3	L1	1.012	1.004	41 ± 5	60 ± 1
	L2	0.992		1	1
	L3	1.000		246 ± 39	—
Sample 4	L1	1.016	1.012	32 ± 6	61 ± 1
	L2	0.994		1	1
	L3	1.000		207 ± 36	—

where F_0 denotes the total formation probability of positronium. $S_{p\text{-Ps}}$, $S_{o\text{-Ps}}$ and S_{e^+} represent the *S* parameter corresponding to *p*-Ps self-annihilation, *o*-Ps pick-off annihilation and free positron–electron annihilation, respectively.

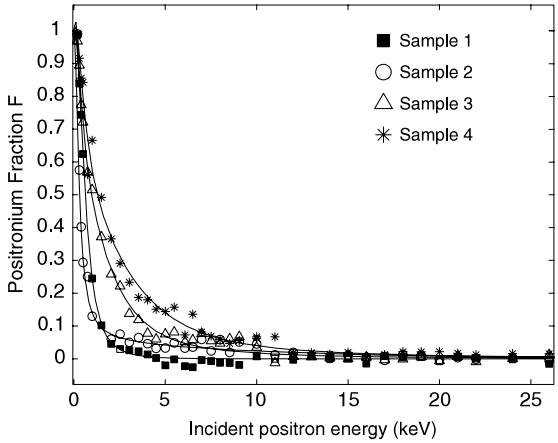

Figure 5. Variation of the positronium fraction versus positron beam energy in the measurement of porous silicon at different anodization conditions.

The VEPFIT analysis shows that all the samples have oxide layers of roughly 60 nm. This layer is formed due to the oxidation of the porous silicon after long exposure to ambient air [40]. The S parameter at the silicon oxide layer S_{oxy} increases from sample 1 to 4. This can be attributed to an increase of p-Ps near the surface. p-Ps has a higher S value compared to $S_{o-\mathrm{ps}}$ and S_{e^+} by virtue of its self-annihilation at thermal energy, and thus will lead to a net increase in S value (equation (7)). With a higher anodization time and current density, the porosity of the sample is expected to increase. The porosity increase would be accompanied by the silicon surface becoming roughened on the atomic scale, making the SiO_2 structure less ordered. The probability of forming p-Ps in the SiO_2 would thus be higher.

Following Asoka-Kumar *et al*, the interface layer is taken as a 1 nm thick absorbing layer [41]. S_{int} exhibits a much lower value than the silicon bulk in all the samples. This effect may be explained by the model proposed by Au *et al* [42], which suggests that S_{int} is significantly influenced by the passivation of the dangling bond at the SiO_2/Si interface. Possible positron trapping centers at the interface are the paramagnetic defect centers (named as the P_{b} centers) that have been observed from ESR measurements at the SiO_2/Si(100) interface [43, 44]. Positrons trapped at the P_{b} centers would predominantly annihilate with the oxygen core electrons, resulting in a lower S_{int} value. If the dangling bonds at the interface are passivated by hydrogen, the S parameter would be expected to become smaller. It is noted (table 2) that S_{int} increases from sample 1 to 4. According to the model of Au *et al*, the interpretation would be a smaller number of hydrogen-passivated dangling bonds. According to the EDX analysis, the amount of oxygen increased from sample 1 to 4 with the dangling bond at the SiO_2/Si interface being stabilized by the formation of the Si–O bond.

4.2.2. $3\gamma/2\gamma$ ratio analysis. The positronium fraction F is plotted as a function of the positron implantation energy in figure 5. At low beam energy a similar value of positronium fraction is obtained in all samples. This is attributed to the formation of Ps at the porous silicon surface and is almost identical for all samples. The positronium fraction remains almost constant for positron beam energies above $E = 11$ keV, indicating that no o-Ps 3γ annihilation is observed. The majority of the positrons annihilate in the silicon substrate with no positronium formation. The sharp increase of the positronium fraction of all samples as the beam energy reduces is due to the increased probability of the intrinsic decay of o-Ps, which is released from

Table 3. Fitting results for the related parameters of the positronium fraction.

Sample number	E_0	n	$L_{o\text{-Ps}}$ (nm)
Sample 1	0.313 ± 0.004	1.61	31
Sample 2	0.382 ± 0.006	1.61	130
Sample 3	1.00 ± 0.003	1.60	210
Sample 4	1.41 ± 0.004	1.60	360

the sample's surface and which then annihilates in the vacuum. The major difference in F can be seen in the energy range from 1 to 10 keV. The value of F in this region increases as the anodization time and current density increases. This remarkable difference can be correlated to the increase of the pore volume or the creation of more pores near the surface of the samples as the anodization time and current density increases.

The profiles of the positronium fraction as a function of positron beam energy are analyzed based on a one-dimensional out-diffusion model, following the studies of out-diffusion of o-Ps from crystalline ice by Eldrup *et al* [45]. By assuming that all the o-Ps which diffuses back to the surface escapes, the fraction of o-Ps diffusing out into the vacuum, F, is described by an empirical expression [45]

$$F(E) = F_0(E)J(E) = \frac{F_0(E)}{1 + (E/E_0)^n}, \tag{8}$$

where $F_0(E)$ is the probability of forming Ps in the sample at positron implantation energy E and $J(E)$ is the fraction of o-Ps diffusing out to the sample surface. $J(E)$ is derived by solving the one-dimensional out-diffusion model for o-Ps in the approximation of an exponential implantation profile.

The mean implantation depth $\langle x \rangle$ is assumed to have the power law relationship [45]

$$\langle x \rangle = AE^n, \tag{9}$$

where E is the implantation energy and A is a constant. The diffusion length of the o-Ps $L_{o\text{-Ps}}$ can be determined by expressing $L_{o\text{-Ps}}$ in terms of an energy E_0

$$L_{o\text{-Ps}} = (\tau D_{o\text{-Ps}})^{1/2} = AE_0^n. \tag{10}$$

The values of E_0 used to fit the $F(E)$ data are listed in table 3. The values of the o-Ps diffusion length were determined by inserting $A = 206$ Å keV^{-n} and the corresponding value of E_0 and n (~ 1.6) into equation (10). It can be clearly observed that the o-Ps diffusion length increases from sample 1 to 4. The increase of the o-Ps diffusion length among the samples indicates an increase of the interconnectivity of open pores, which increases with the higher current density and longer anodization times. This signifies that the o-Ps in the porous silicon fabricated with higher current density and etching time travels longer distances to diffuse back out into the vacuum. The fact that the Ps diffusion length is larger than the positron diffusion length suggests the presence of open pores on the sample's surface. The results also suggest that the analysis of the o-Ps diffusion length can be technologically important because it provides valuable information with respect to the open pore interconnectivity of the porous media.

4.3. CDBS analysis

Due to its low peak to background ratio in the high momentum region, coincidence Doppler broadening spectroscopy (CDBS) has proved to be useful in identifying the chemical surroundings of the annihilation site [46–48]. To further enhance the effective instrumental resolution, we have applied deconvolution using the Richardson–Lucy (RL) algorithm to the

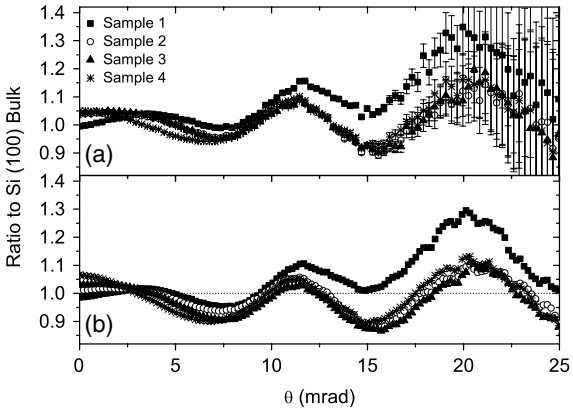

Figure 6. Non-deconvoluted (a) and deconvoluted (b) positron–electron momentum ratio curves for porous silicon, referenced to crystalline n-type silicon.

annihilation spectra [49]. In the deconvolution process, the measured CDBS data g is described as a convolution of the true function f with the instrument's PSF (point spread function) h

$$g = h \otimes f + n, \tag{11}$$

where n is the statistical noise. The true function f is determined iteratively via the expression [50, 51]

$$f_{k+1} = f_k \left[h * \frac{g}{h \otimes f_k} \right] \triangleq \hat{O}_{\mathrm{RL}}(f_k), \tag{12}$$

where f_k is the estimate of f after k iterations and $*$ is the correlation operator and $\hat{O}_{\mathrm{RL}}$ is the RL operator. Details of the deconvolution using the RL algorithm have been reported in [49].

The positron–electron momentum ratio curves referenced to n-type (100) silicon obtained from the RL deconvoluted CDBS spectra are shown in figure 6. Although these curves are taken using a ^{22}Na source, a significant fraction of positrons annihilate in the porous region. This is because the mean positron penetration depth is $\sim$120 μm which is commensurate with the porous silicon width (36–146 μm, table 1).

The ratio curves reveal a similar shape of annihilation momentum distribution for all the samples. This suggests that the samples exhibit a high degree of structural similarity and that the electrochemical anodization does not have a significant change on the sample's chemical environment. Characteristic ratio peaks appear around $p_{\mathrm{L}} \approx 12$ mrad and $\approx$20 mrad. These can be attributed to positron annihilation with the oxygen core electrons [52]. The amplitude of these peaks reflects the number of oxygen impurity atoms around the pore and interface. The W parameters determined from the annihilation spectra are shown in table 4. They decrease gradually from sample 1 to 4, indicating a decrease of positrons annihilating with the oxygen core electrons. The most likely explanation of this is that p-Ps and positrons confined in the pore are more confined in the low porosity samples leading to more Doppler broadening. Moreover, hydrogen passivation would also lead to more oxygen core annihilation events in low porosity samples.

4.4. Lifetime analysis

PALS spectra obtained for the porous Si samples are shown in figure 7. The results were first analyzed using the POSITRONFIT [53] software from which the lifetime spectrum is described

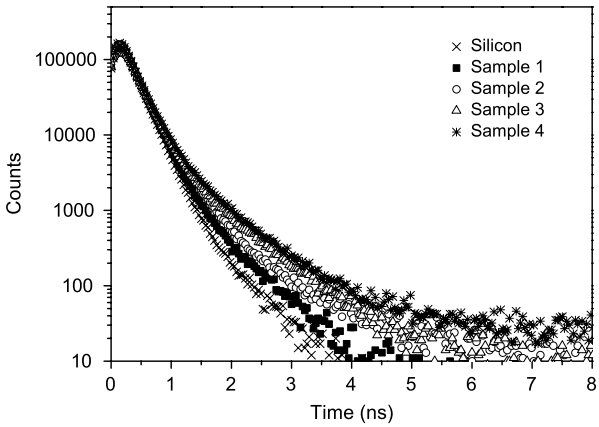

Figure 7. Positron lifetime spectra of the silicon under different electrochemical etching conditions.

Table 4. Fitting results of the positron lifetime components in porous silicon by POSITRONFIT. The S and W parameters are determined from the CDBS experimental results.

Sample number	τ_1 (ns)	I_1 (%)	τ_2 (ns)	I_2 (%)	τ_3 (ns)	I_3 (%)	Pore size (nm)	S/S_{Si}	W/W_{Si}
Sample 1	0.218	67	0.439	32	2.062	1.0	1.37	1.0005	0.90
Sample 2	0.218	56	0.483	42	2.098	1.5	1.41	1.0149	0.85
Sample 3	0.218	54	0.462	44	2.132	1.9	1.41	1.0279	0.82
Sample 4	0.218	52	0.467	45	2.227	2.7	1.51	1.0407	0.80

as a sum of discrete exponentials

$$s(t) = \sum_i I_i \lambda_i \exp[-\lambda_i t], \tag{13}$$

where I_i is the intensity of a positron in the ith stationary positron state with decay rate λ_i. The fitting results of the lifetime spectra are shown in table 4. The analyzed results show that three characteristics lifetimes can been resolved in each sample. All the samples show a clear long lifetime (∼2 ns) in the spectrum. This long-lived lifetime component can be attributed to the *o*-Ps pick-off annihilation. There is also an intermediate lifetime component of about 0.48 ns that is most likely attributed to positrons annihilating at the SiO_2/porous silicon interface. The shortest positron lifetime of 218 ps is due to annihilation in the bulk silicon [54]. This value is kept fixed during fitting. The *p*-Ps component has been neglected in the analysis since from the I_3 measurements (table 4) its intensity is expected to be ∼0.3–1.0%.

The long-lived component intensity of the porous silicon, I_3, increases with the anodization current density and time but the longest lifetime τ_3 does not change significantly. τ_3 may be attributed to ortho-positronium (*o*-Ps) localized in the micropores. As such, it depends on the free volume size at the pore and the slight increase from sample 1 to 4 suggests an increase in the pore size with etching. Moreover, the increase of *o*-Ps intensity I_3 indicates the increase of pore concentration. An increase in the intensity (I_3) of intermediate lifetime τ_2 is also observed. This is probably due to an increased fraction of positrons annihilating with the oxide layer on the porous silicon surface or on its interface with silicon.

To further characterize the pore size distributions in the samples and verify the POSITIONFIT fitting results, the lifetime spectra were also analyzed using the Laplace inversion program CONTIN-PALS2 [55, 56]. In this analysis the positron lifetime spectrum

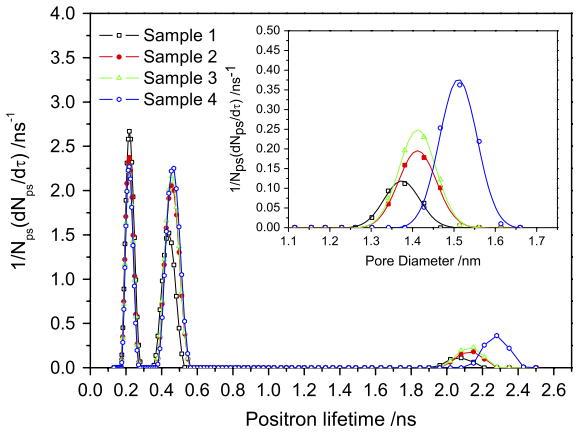

Figure 8. Probability density functions (PDF) as a function of positron lifetime, resulting from a lifetime spectra analysis using CONTIN-PALS2. Inset: PDF as a function of pore size calculated via the Tao–Eldrup equation (equation (5)).

(This figure is in colour only in the electronic version)

is represented by a continuous decay of the form

$$s(t) = \int_0^\infty \lambda a(\lambda) \exp(-\lambda t)\, \mathrm{d}\lambda = L\lambda a(\lambda), \tag{14}$$

where $\int \lambda(a)\, \mathrm{d}\lambda = 1$ [57]. The results of the analysis are shown in figure 8 as positron lifetime probability distributions. The pore size distributions (PSDs) shown in the insert of figure 8 are determined from the positron lifetime distributions using equation (5). In doing this the free volume sizes of the micropores as seen by the positronium are assumed spherical. From table 4 and figure 8 the mean pore diameter from ∼1.37 to ∼1.51 nm under the increased etching time and current density is seen to increase from sample 1 to 4. This agrees with the well known increase in porosity seen in porous Si as seen in TEM.

4.5. Photoluminescence study

Figure 9 shows the PL spectra under 325 nm laser excitation at room temperature. It can be observed that the samples exhibit visible emission in two distinct bands. The luminescence of samples 1 and 2 shows strong blue-green emission in the F band, while the PL spectra of samples 3 and 4 reveal a red-blue (S band) emission with a relatively large bandwidth. For samples 1 and 2, the PL spectra can be well fitted by three Gaussian peaks lying in the range 2.79–3.01 eV (411–444 nm) with FWHMs in the range 0.11–0.43 eV. The large bandwidth of the PL spectra of samples 3 and 4 can be fitted using a single Gaussian peak. The peak positions are at 1.71 eV (725 nm) and 1.74 eV (713 nm).

The origin of the visible luminescence in porous silicon is still controversial. It is, however, generally accepted that the luminescence originates from quantum confinement together with the effect of surface passivation. Wolkin *et al* [17] studied the electronic states in Si nanocrystals as a function of cluster size and surface passivation based on electronic structure calculations. The electronic states in porous silicon were characterized in three zones depending on the size of the Si nanocrystallite. For size larger than ∼2.9 nm (zone I), the PL mechanism can be understood by quantum confinement. As the nanocrystallite size decreases to zone II (∼1.9 nm $<$ ∼2.9 nm), the effect of recombination involving a free hole and a

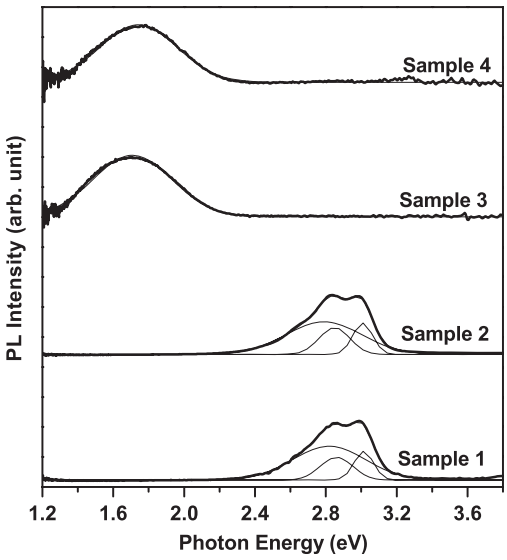

Figure 9. Room temperature PL spectra of porous silicon under different anodization conditions.

trapped electron may be slowed down by surface passivation. When the cluster size is smaller than ∼1.9 nm (zone III), the surface passivation effect dominates and results in a huge redshift in the PL spectrum. Theoretical studies on the porous silicon structural configuration seem to agree with Wolkin's interpretation. Luppi *et al* [58, 59] studied the influence of the Si=O double bond on the electronic bandgap through *ab initio* calculations. The results show that the first Si=O double bond formed at the micropore surface originates a huge reduction in the energy gap. When more Si=O double bonds are formed, a further reduction of the bandgap is introduced but is weaker than the first Si=O double bond. The contribution of the Si=O bonds to the bandgap weakens as the density of the double bond is increased.

According to the model proposed by Wolkin *et al*, the blue-green emission observed in samples 1 and 2 can be understood as arising from quantum confinement and bandgap widening [17, 60, 61]. The presence of multiply resolved peaks in samples 1 and 2 on this model is due to variation in the bandgap energy caused by the wide range of micropore sizes. Moreover, from the τ_3 results the micropores in the present study are typically 1.4 nm in diameter indicating the zone III regime. The sudden switch to red light emission in samples 3 and 4 can be understood from this observation that the micropore size is in zone III, since in this region the effect of Si=O double bond formation is significant. The emission of red light is thus due to the additional effect of oxygen coverage on the porous silicon surface, causing an increase in the number of Si=O double bonds formed at the SiO_2/Si interface. This is supported by the EDX measurements from which the presence of oxygen atoms was found to increase from sample 1, suggesting a increase in Si=O double bonds at the interface with the accompanying removal of dangling bonds. The Si=O formed provide trapped surface states that reduce the effective size of the optical gap and result in the red band emission.

4.6. Correlation between PL and PAS studies

It is clear from the PAS study (section 4.2.1) and the PL study (section 4.5) that a strong correlation exists between the data taken from each technique. A sudden switching in the

SiO_2 S parameter S_{oxy} occurs between samples 1/2 and samples 3/4, with the S parameter at the SiO_2 layer of samples 1 and 2 showing a much lower value than that of samples 3 and 4 (figure 3). Thus the distinct switching optical behavior of these samples is correlated with that seen in the S parameter. Since it is found from the PALS study that the fraction of positrons forming Ps is small (∼2% of the total annihilation), the sudden switching cannot be due to changes in Ps formation. The diffusion length of positrons in Si is ∼200 nm, which is much greater than the inter-pore spacing in the SiO_2 and Si. It follows that essentially all positrons will annihilate from the Si/SiO_2 interface internal to the micropores. The present results suggest then that some sudden change occurs in the structure of the Si/SiO_2 interface. As discussed in section 4.5 the switching action in the PL, as shown by Luppi *et al*, is most probably due to the formation of saturated Si=O double bonds as suggested by Luppi *et al*. The formation of Si=O bonds reduces H-passivated dangling bonds in samples 3 and 4 significantly, which may result in the positron less preferentially annihilating with the oxygen core electron, causing a higher value of S_{oxy} as discussed in section 4.2.1

5. Summary and conclusion

In this work, porous silicon samples fabricated under different anodization current densities and etching times which have been exposed to air, have been characterized using SEM, positron annihilation spectroscopy and photoluminescence. SEM reveals the presence of micropores and macropores on the silicon surface with thicknesses varying from 40 to 140 μm according to anodization conditions. EDX analysis reveals an increase of oxygen near the surface of the samples with anodization current and etching time. Depth profiling of the positron and positronium annihilation parameters has been carried out. The Ps diffusion length is found to be substantially larger than the positron diffusion length indicating a large open pore interconnectivity. The Ps diffusion length increases for increased anodization current and etching time, demonstrating a higher porosity as expected. The size of the micropores in the porous silicon matrix has been determined from the studies of the positronium lifetime using PALS. The average size of the micropores (1.37–1.51 nm) was found to increase with the anodization conditions. The PL spectra studies on the samples revealed visible luminescence in two distinct bands. The blue luminescence of the samples is considered to be due to the transitions of the confined electrons in the nanocrystalline structure and the red emission is attributed to the indirect transition of electron states caused by the Si=O double bond in the SiO_2 layers. The distinct behavior in PL has been correlated with the switching action of the S parameter observed in the SiO_2 layer in VEDBS measurements. Both of these phenomena suggest that the formation of Si=O bonds reduces hydrogen-passivated dangling bonds resulting in a higher value of S parameter in the SiO_2 layer. It has been argued that this passivation can also explain the decrease in the oxygen peak in the CDBS spectra with positrons being less able to interact with oxygen core electrons in the Si=O state.

Acknowledgments

This work was supported by the Research Grants Council of The Hong Kong Special Administrative Region, China (project nos HKU 7004/04P and HKU 7004/07P).

References

[1] Uhlir A 1956 *Bell Syst. Tech. J.* **35** 333
[2] Canham L T 1990 *Appl. Phys. Lett.* **57** 1046
[3] Jung K H, Shih S and Kwong D L 1993 *J. Electrochem. Soc.* **140** 3046

[4] Bondarenko V P and Yakovtseva V A 1997 *Properties of Porous Silicon* ed L T Canham (London: Inspec) pp 356–61
[5] Buttard D, Bellet D and Baumbach T 1996 *Thin Solid Films* **276** 69–72
[6] Dian J, Macck A, Ňanský D N, Němec I, Vrkoslav V, Chvojka T and Jelinek I 2004 *Appl. Surf. Sci.* **238** 169
[7] Fauchet P 1991 *Light Scattering in Semiconductor Structures and Superlattices* ed D J Lockwood and J F Young (New York: Plenum) p 229
[8] Libon I, Voelkmann C, Petrova-Koch V and Koch F 1997 *Mater. Res. Soc. Symp. Proc.* **452** 511
[9] Mizuno H, Koyama H and Koshida N 1996 *Appl. Phys. Lett.* **69** 3779
[10] Kovalev S I, Yaroshetzkii I D, Muschik T, Petrova-Koch V and Koch F 1994 *Appl. Phys. Lett.* **64** 214
[11] Chen Q W, Zhu D L, Zhu C, Wang J and Zhang Y G 2003 *Appl. Phys. Lett.* **82** 1018
[12] Cullis A G, Canham L T and Calcott P D J 1997 *Appl. Phys. Rev.* **82** 3
[13] von Behren J, Buuren T V, Zacharias M, Chimowitz E H and Fauchet P M 1998 *Solid State Commun.* **105** 317
[14] Schuppler S *et al* 1995 *Phys. Rev.* B **52** 4910
[15] Herino R 1997 *Properties of Porous Silicon* ed L T Canham (London: Inspec) p 3
[16] Canham L T 1997 *Properties of Porous Silicon* ed L T Canham (London: Inspec) pp 88–97
[17] Wolkin M V, Jorne J and Fauchet P M 1999 *Phys. Rev. Lett.* **82** 197
[18] Itoh Y, Murakami H and Kinoshita A 1993 *Appl. Phys. Lett.* **63** 22
[19] Biasini M, Ferro G, Monge M A, Francia G D and Ferrara V L 2000 *J. Phys.: Condens. Matter* **12** 5961
[20] Knights A P, Kowalski G, Saleh A S, Towner A, Patel M I, Rice-Evans P C, Moore M and Gledhill G A 1995 *J. Appl. Phys.* **78** 7
[21] Suzuki R, Mikado T, Ohgaki H, Chiwaki M and Yamazaki T 1994 *Phys. Rev.* B **49** 17484
[22] Dannefaer W S, Wiebe C and Kerr D 1998 *J. Appl. Phys.* **84** 12
[23] Coleman P 2000 *Positron Beams and Their Applications* (Singapore: World Scientific) pp 41–86
[24] Gidley D W, Peng H G and Vallery R S 2006 *Annu. Rev. Mater. Res.* **36** 49
[25] Weber M H and Lynn K G 2003 *Principles and Applications of Positron and Positronium Chemistry* ed Y C Jean, P E Mallon and D M Schrader (Singapore: World Scientific) chapter 7, p 167
[26] Brusa R, Macchi C, Mariazzi S and Karwasz G 2005 *Acta Phys. Pol.* A **107** 4
[27] Ito K and Kobayashi Y 2005 *Acta Phys. Pol.* A **107** 5
[28] Petkov M P, Wang C L, Weber M H, Lynn K G and Rodbell K P 2003 *J. Phys. Chem.* B **107** 2725
[29] Lynn K G and Welch D O 1980 *Phys. Rev.* B **22** 99
[30] Eldrup M, Lightbody D and Sherwood J N 1981 *Chem. Phys.* **63** 51
[31] Jean Y C 1990 *Microchem. J.* **42** 72
[32] Nakanishi H, Wang S J and Jean Y C 1988 *Positron Annihilation Studies of Fluids* (Singapore: World Scientific) p 292
[33] Consolati G 2002 *J. Chem. Phys.* **117** 15
[34] Cao H, Zhang R, Sundar C, Yuan J, He Y, Sandreczki T, Jean Y and Nielsen B 1998 *Macromolecules* **31** 6627
[35] Zhang R, Gu X, Chen H, Zhang J, Li Y, Nguyen T, Sandreczki T C and Jean Y 2004 *J. Polym. Sci.* B **42** 2441
[36] Hossain S, Das J, Chakraborty S, Dutta S and Saha H 2002 *Semicond. Sci. Technol.* **17** 55
[37] Cheung C K, Naik P S, Beling C D, Fung S and Weng H M 2006 *Appl. Surf. Sci.* **252** 3132
[38] van Veen A, Schut H, Vries J D, Hakvoort R, Ijpma M, Schultz P, Massoumi G and Schultz P J (ed) 1990 Positron beams for solids and surfaces *AIP Conf. Proc.* **128** 171
[39] Ito K and Kobayashi Y 2005 *Acta Phys. Pol.* A **107** 5
[40] Canham L T, Houlton M R, Leong W Y, Pickering C and Keen J M 1991 *J. Appl. Phys.* **70** 422
[41] Asoka-Kumar P, Lynn K G and Welch D O 1994 *J. Appl. Phys.* **76** 4935
[42] Au H L, Asoka-Kumar P, Nielsen B and Lynn K G 1992 *J. Appl. Phys.* **73** 15
[43] Poindexter E H and Caplan P J 1983 *Prog. Surf. Sci.* **14** 201
[44] Nishi Y 1971 *Japan. J. Appl. Phys.* **10** 52
[45] Eldrup M, Vehanen A, Schultz P J and Lynn K G 1985 *Phys. Rev.* B **32** 7048
[46] Alatalo M, Kauppinen H, Saarinen K, Puska M J, Makinen J, Hautojarvi P and Nieminen R M 1995 *Phys. Rev.* B **51** 4176
[47] Alatalo M, Barbiellini B, Hakala M, Kaupinen H, Korhonen T, Puska M J, Sarrinen K, Hautojarvi P and Nieminen R M 1996 *Phys. Rev.* B **54** 2397
[48] Myler U and Simpson P J 1997 *Phys. Rev.* B **56** 14303
[49] Zhang J D, Zhou T J, Cheung C K, Beling C D, Fung S and Ng M K 2006 *Nucl. Instrum. Methods* A **560** 552
[50] White R L 1994 *Astronomical Data Analysis Software and System III* (*ASP Conf. Seris* vol 61) p 292
[51] Biggs D S C and Andrews M 1997 *Appl. Opt.* **36** 1766
[52] Tang Z, Nonaka T, Nagai Y and Hasegawa M 2001 *Mater. Sci. Forum* **67** 363
[53] Kirkegaa P and Eldrup M 1974 *Comput. Phys. Commun.* **7** 401

[54] He Y J, Hasegawa M, Lee R, Berko S, Adler D and Jung A-L 1986 *Phys. Rev.* B **33** 5924
[55] Provencher S W 1982 CONTIN version 2DP *Comput. Phys. Commun.* **27** 213
[56] Gregory R B and Zhu Y 1990 *Nucl. Instrum. Methods Phys. Res.* A **290** 182
[57] Shukla A, Peter M and Hoffmann L 1993 *Nucl. Instrum. Methods* A **335** 310
[58] Ossicini S, Degoli E, Luppi M and Magri R 2002 *SPIE* **4808** 73
[59] Luppi M and Ossicini S 2003 *Phys. Status Solidi* **197** 251
[60] Kanemitsu Y 1995 *Phys. Rep.* **263** 1
[61] Kanemitsu Y, Futagi T, Matsumoto T and Mimura H 1994 *Phys. Rev.* B **49** 14732